Higher Harmonics in Multipactor Induced Plasma Ionization Breakdown near a Dielectric Surface

De-Qi Wen, Peng Zhang, Janez Krek, Yangyang Fu, and John P Verboncoeur

Higher Harmonics in Multipactor induced Plasma Ionization Breakdown Near a Dielectric Surface

De-Qi Wen[1,2], Peng Zhang[1], Janez Krek[2], Yangyang Fu[3], John P Verboncoeur[1,2]

[1]*Department of Electrical and Computer Engineering, Science and Engineering,*
Michigan State University, East Lansing, MI 48824, USA
[2]*Department of Computational Mathmatics, Science and Engineering,*
Michigan State University, East Lansing, MI 48824, USA and
[3]*Department of Electrical Engineering, Tsinghua University, Beijing, 100083, China*

In this letter, the novel physics of higher harmonic (HH) generation of the normal electric field near a dielectric surface is reported in multipactor induced plasma ionization breakdown, as determined by kinetic particle-in-cell (PIC) simulations. The observed HH frequency is around ten times the fundamental rf driving frequency, but lower than the electron plasma frequency. A theory is constructed which indicates that stream plasma interaction-induced instability is the mechanism of HH generation in the collisional regime. The HH frequency and its corresponding growth rate of the HH oscillation amplitude from the theory are in good agreement with kinetic PIC simulations.

Multipactor [1, 2] is a vacuum discharge based on secondary electron emission (SEE). When the SEE yield is repeatedly above the unity, an avalanche of electrons exposed to rf electric field on a dielectric surface or between two metal surfaces appears. In the presence of background gas, multipactor will trigger gas ionization breakdown. Multipactor and plasma discharge are of importance in many fields, including rf accelerators in particle and nuclear physics [3], rf plasma source in material processing [4–6], space plasma and propulsion, fusion energy, high voltage insulators from DC to microwaves, higher power microwave systems and space-based satellite communications [1, 2, 7–11]. In high power microwaves and space-based communications, multipactor and gas discharges near rf windows have also been the key limiting factors [1, 7, 12–15]. Therefore, understanding the fundamental physics of such a widely present configuration involving ionization breakdown and electron-surface multipacting process is essential.

Multipactor discharge is the dominant process in less collisional regime [1, 12, 15], and its susceptibility [1, 13, 16, 17], temporal evolution [18–20], and mitigation [21–25] have been comprehensively investigated. However, in the presence of frequent electron-neutral impacts due to background or evaporated gas from the surface, multipactor dynamics can be significantly altered via electron-neutral momentum transfer collisions and energy loss [26]. In the limit of near-atmospheric pressure, the electron energy loss is significant during flight, and the remaining impact energy on the surface is insufficient that the surface multipactor is fully suppressed over time [27], and the plasma reaction and transport dynamics become dominant [7, 28, 29]. In the pressure range from hundreds of mTorr to a few Torr, both plasma discharges and surface multipactor can exist [27, 30]. Lau *et al* [31] theoretically investigated the scaling laws for discharge formation time under a spatially uniform electric field. Understanding the fundamental transient physics regarding the electron-surface multipacting and gas ionization is a crucial step for researchers to control the discharge,

but it is barely studied due to the experimental limitation of resolution in time and space, as well as the computational cost for fully kinetic simulation.

In this Letter, we report the novel physics of higher harmonic (HH) generation in multipactor-coexisting plasma ionization breakdown at intermediate pressure (hundreds of mTorrs). Kinetic particle-in-cell (PIC) simulations, which are well benchmarked [32–34] and validated by experiments [35] in plasma discharges, are conducted and a theory is constructed, which reveals the nature of HH generation. To reveal the fundamental physics, in this work, we mainly present a typical case at frequency $f = 1\,\mathrm{GHz}$, which is commonly used in space-based communication system, and background argon pressure $0.2\,\mathrm{Torr}$ close to that suggested by recent multipactor breakdown experiments [15].

The schematic of the discharge system is shown in Fig. 1, where the discharge is bounded by a dielectric surface at $x = 0$. The right boundary is free space and far away from the discharge. At the early stage of gas ionization breakdown, the electron density is low, and a rf electric field tangential to the surface is employed as adapted by Lau *et al* [31] and Zhang *et al* [36]. As shown in Fig. 1, the tangential sinusoidal electric field has an amplitude of $E_{\mathrm{rf0}} = 3\,\mathrm{MV/m}$. The interactions between charged and
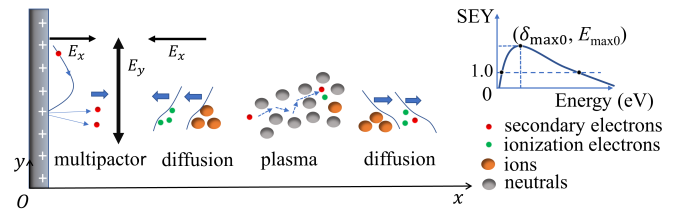

FIG. 1: Schematic of the system for multipactor induced ionization breakdown in fully kinetic particle-in-cell simulations. The small zoomed plot qualitatively shows the secondary electron yield (SEY), δ, as a function of electron impact energy for normal incidence.

neutral particles are treated by a standard Monte-Carlo scheme incorporating the null collision method [37, 38]. The details about the reaction threshold and cross sections can be found in [39–44]. The time step and grid size is 10^{-14}s and $0.175\,\mu$m, respectively, an initial electron current at $1.3\,$kA/m^2 is emitted for the first rf period [18]. The charged particles flowing to the dielectric surface cause charge accumulation. Electron transport is self-consistently considered [45, 46]. The secondary electron emission from surface induced by primary electron impacts is described by the well-known Vaughan empirical formula [47] for a dull surface of silicon oxide, which is a typical material for rf windows [1].
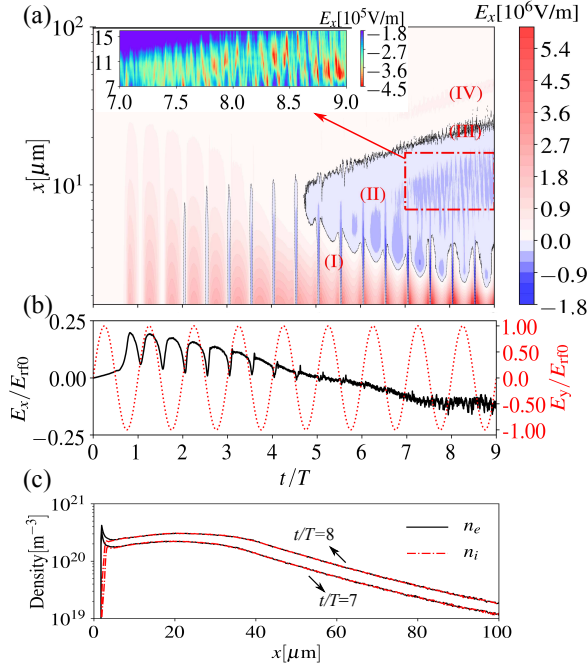

FIG. 2: Spatiotemporal plots of the (a) normal electric field, E_x, (b) the normalized rf electric field (red dashed line), E_y/E_{rf0}, and normal electric field, E_x/E_{rf0} at $x = 12\mu$m, (c) the spatial plots of electron and ion density at $t/T = 7, 8$.

Fig. 2(a) shows the spatiotemporal normal electric field, E_x, which increases rapidly at the beginning due to the secondary electron avalanche emission from the surface, and then periodically oscillates at twice the fundamental rf frequency (1 GHz), similar to the multipactor process in vacuum [18, 19]. The normal electric field points away from the surface everywhere and gradually decays in space due to space charge neutralization. E_x/E_{rf0} at the specific location $x = 12\mu$m is exhibited in Fig. 2(b), in which the red line denotes temporal E_y/E_{rf0}. Most importantly, remarkable fast oscillations in time, i.e., HHs of the normal electric field (as well as other plasma parameters, see later) are observed, which have never been found before. In order to explicitly display these oscillations, a local plot of electric field within the red box in Fig. 2(a) is shown in the subplot. We can see that oscillation frequency of the HH is around

10 GHz, much higher than the fundamental frequency and lower than the electron plasma frequency f_{pe} (around 10^2 GHz). The oscillations roughly start from the sixth period and becomes stronger in time (see Fig. 2(b)). In vacuum multipactor discharges, there is no enhanced HH frequency spectrum [48, 49]. Additionally, the fast oscillating E_x mainly locates in the transition region (region (II)) from multipactor-dominant region (region (I)) to the plasma region (region (III)), and appears slightly in the plasma region (III) and (IV). The typical length of the region where the longitudinal oscillating electric field appears is around $20\,\mu$m. The black dashed line in Fig. 2(a) shows the contour value of $E_x = 0$ V/m, which indicates the boundaries among regions (I)-(IV), i.e., the multipactor region (I) with $E_x > 0$, the transition region (II) with $E_x < 0$ and main plasma region (III) $E_x \approx 0$, and region (IV) $E_x > 0$. The multipactor region (I) is gradually depressed because plasma grows in time, as the increasing ion density (dashed line) shows in Fig. 2(c) for $t/T = 7$ and 8, respectively.

The electron density n_e as shown in Fig. 2(c) is significantly higher than the ion density near the surface because the primary electrons impact the surface and induce intense secondary electron emission, that mainly localizes near the surface; additionally, more and more electrons are created due to abundant electron-neutral ionization impacts in the plasma region (III), and diffuse towards the surface. Different from a pure ion sheath surrounding plasma, within which electric field points towards surface from plasma, here, this local high negative electron charge results in positive electric field in region (I) and negative electric field in region (II). The ions move collectively and slowly and are not modulated by the HHs of the electric field since $f_{HH} \gg f_{pi}$.

We analyze the nature of this HH generation based on simulation data of the breakdown process and a theoretical model. The ion is almost immobile over an rf period due to its large mass. Therefore, the appearance of HHs on small time scales is linked to electron dynamics. We label the electrons in simulation by two different generation sources: the electrons from ionization impacts are labeled as ionization electrons (ie) and those emitted from the surface are labeled as secondary electrons (se), whose spatiotemporal plots of density are shown in Fig. 3(a) and (b), respectively. Again, remarkable HH oscillations are observed for both ie and se. The corresponding electron fluid velocity also shows similar behaviors (not shown here). The corresponding velocity distribution functions for ie and se, $f(u_{ie})$ and $f(u_{se})$, are measured in the PIC simulation. It is worth noting that the velocity distribution profiles are roughly the same near $x = 12\mu$m, and over a time interval $7 < t/T < 9$. Here, we show the typical results for ie and se in Fig. 3(c) for $x = 12\,\mu$m and $t/T \approx 7$. The ionization electrons have a small net negative fluid velocity $v_{ie0} = \int_{-\infty}^{+\infty} u_{ie} f(u_{ie}) du_{ie} \approx -1.16 \times 10^5$m/s, implying that the ie flows towards the dielectric surface. The secondary electron distribution function shows two narrow
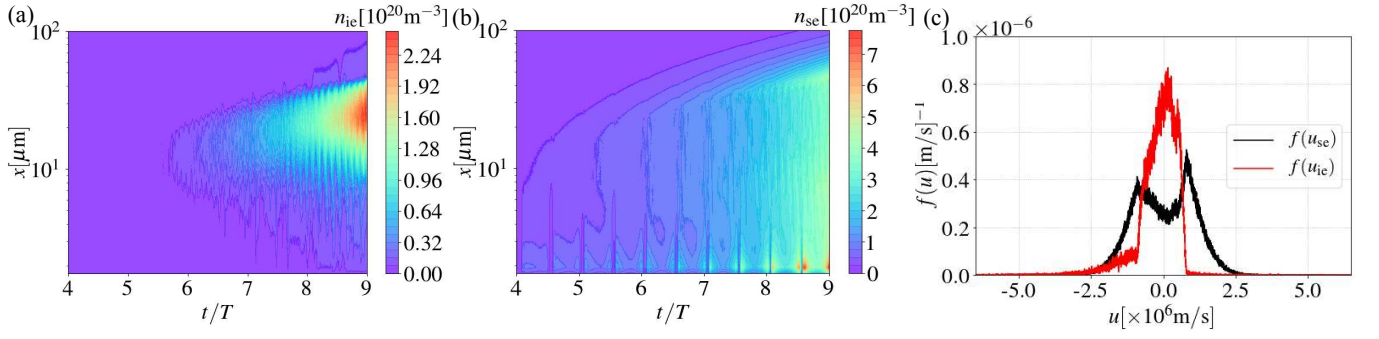
FIG. 3: The spatiotemporal plots of the (a) electron density from ionization impact and (b) secondary electron density from the surface emission; (c) the velocity distribution functions at $x = 12\mu$m of the ionization and secondary electrons normalized to each species density.

peaks, i.e., some secondary electrons ($u_{se} > 0$) are injecting into the plasma and the others ($u_{se} < 0$) are leaving the plasma for the surface. For the group of secondary electrons with $u_{se} > 0$, the distribution function is approximated by a Dirac δ-function, enabling us to model it as a cold electron stream, which will interact with ionization electrons in the plasma. In the following, the cold stream-plasma interaction is theoretically modeled by describing the ionization and secondary electrons as fluids. The background ions are immobile as discussed above, and the surface charge-induced restoring field is shielded by the dense electrons near the surface, and it is assumed to have little effect on the stream-plasma interaction.

In the following, the fluid velocity and density of ionization and secondary electrons are denoted by subscripts ie and se, respectively. Within the time duration of a few HH oscillations, the electron density is assumed unaffected by impact ionization. For ionization electrons, the density n_{ie} and fluid velocity v_{ie} follow the continuity equation with the net volume source set to zero,

$$\frac{\partial n_{ie}}{\partial t} + \frac{\partial v_{ie} n_{ie}}{\partial x} = 0 \qquad (1)$$

The ionization electrons also satisfy momentum balance

$$\frac{\partial v_{ie}}{\partial t} + v_{ie}\frac{\partial v_{ie}}{\partial x} = -\frac{e}{m}E_x - \frac{1}{n_{ie}}\frac{\partial p_{ie}}{\partial x} - \nu_m v_{ie} \qquad (2)$$

where E_x is the space charge-induced normal electrostatic field, $\partial p_{ie}/\partial x = \partial(n_{ie}k_B T_x)/\partial x$, and ν_m is the effective electron-neutral momentum transfer frequency. The longitudinal electrostatic field, $E_x = -\partial\phi/\partial x$, follows Poisson's equation $\partial^2\phi/\partial x^2 = -\rho/\epsilon_0$ with ϕ the potential in space, ϵ_0 the permittivity of vacuum and ρ the charge density.

We define a general time-dependent physical quantity A, representing the ionization electron fluid velocity and density, as well as the potential, and split it into two terms, $A = A_0 + \delta A$, where A_0 denotes the slowly varying quantity driven by the fundamental frequency field, and the second term $\delta A = \tilde{A}e^{j(kx - \omega t)}$, describes a fast longitudinal oscillation at angular frequency ω and wavenum-

ber k. Thus, the growth of the perturbation and frequency of oscillations in time are described by the imaginary and real part of ω, respectively. k is a real number, i.e., the oscillations grow in time only. Replacing A by n_{ie}, v_{ie}, and ϕ, separately, and inserting it into Eqs. (1)-(2), neglecting the second order terms (i.e., linearizing), we can express n_{ie} as a function of $\tilde{\phi}$.

$$\tilde{n}_{ie} = \frac{ke\tilde{\phi}/m}{\frac{(-\omega + kv_{ie0} - jv_{em})(\omega - kv_{ie0})}{kn_{ie0}} + \frac{kk_B T_x}{n_{ie0}m}} \qquad (3)$$

For secondary electrons injecting into plasma treated as a cold stream, the pressure gradient and collisional term are omitted, similarly to Eq. (3), we have

$$\tilde{n}_{se} = \frac{ke\tilde{\phi}/m}{(-\omega + kv_{se0})(\omega - kv_{se0})/kn_{se0}}. \qquad (4)$$

Substituting Eqs. (3) and (4) into Poisson's equation, finally we obtain the dispersion equation describing the relationship of frequency and growth rate of oscillation and the wavenumber in the collisional stream-plasma interaction system

$$1 = \frac{\omega_{ie0}^2}{(\omega - kv_{ie0} + jv_{em})(\omega - kv_{ie0}) + k^2 k_B T_x/m} + \frac{\omega_{se0}^2}{(\omega - kv_{se0})(\omega - kv_{se0})} \qquad (5)$$

where $\omega_{ie0,se0}^2 = e^2 n_{ie0,se0}/m\epsilon_0$. From the measurements in PIC simulations near $t/T \approx 7$, the ionization electron density $n_{ie0} = 3 \times 10^{19}$m^{-3}, and velocity $v_{ie0} = -1.16 \times 10^5$m/s, and the secondary electron density $n_{se0} = 5 \times 10^{19}$m^{-3} and the secondary electron velocity $v_{se0} = 10^6$ m/s. The effective ionization electron momentum transfer frequency is collected from PIC simulation and has a value of $\nu_m = 0.7 \times 10^9$s^{-1}. T_x corresponds to the x component of the pressure tensor diagonals measured from simulation [50, 51]. Solving Eq. (5) gives the oscillating angular frequency ω versus wavenumber k. If the ionization electrons are treated as cold electrons [52] and electron-neutral collisions are

absent [53], then Eq. (5) reduces to the classical dispersion relationship for two stream instabilities [54]. We stress that, different from the classical two-stream theory in [54], the term of $k^2 k_B T_x/m$ in Eq. (5) here is important to give the correct growth rate of HH oscillations, as the assumption of cold ionization electrons ($T_x = 0$) is found to result in a much higher growth rate than measured in PIC simulations. The secondary electron stream leaving the bulk plasma ($u_{se} < 0$) moves in the same direction as ionization electrons, thus it is less important and has been excluded.

Fig. 4(a) exhibits the variation of complex ω versus wavenumber k in Eq. (5). The left and right vertical axes denote the real and imaginary part of ω, Re(ω) (black line) and Im(ω) (red line), respectively, and the vertical blue dashed line indicates the maximum Im(ω), whose wavenumber, k_{max}, reveals the dominant longitudinal oscillation mode [54–56]. The corresponding Re(ω) at k_{max}, gives the oscillation frequency of around 10 GHz, in very good agreement with the kinetic simulation. Meanwhile, we obtain a longitudinal oscillation at wavelength 11 μm, which is very close to simulation again. In addition, the secondary electron velocity distribution function (Fig. 3(c)), $f(u_{se})$, has a small broadening compared to an ideal Delta function, therefore, the response of the wavenumber and oscillation frequency to both the shift of the drift velocity and electron density is examined. It turns out the results are robust at slightly varying input parameters within ±10%. The contour plot of Fig. 4(b) shows the temporal spectrum of the normal electric field from the PIC simulation over 1.6 rf period at near $x = 12\mu m$. We can see the most significant components of the HH locate around 10 GHz. The brightness of the color bar represents the strength of the magnitude at the corresponding frequency. The second harmonic frequency [18, 19] is also captured due to the collective response of electrons to the rf electric field, i.e. the electrons 'see' the strength rather than the phase of the rf transverse electric field between two electron-neutral collisions. Based on Eq. (5), theoretical calculation of the oscillation frequency by importing the unperturbed electron fluid velocity, density, and electron temperature from simulation gives the rectangle line with error bars in Fig. 4(b). The required secondary/ionization electron fluid velocity and density is obtained by filtering the higher frequency oscillations. The error bars are obtained by varying the ionization electron drift velocity $v_{ie0} \pm 10\%$. The time-dependent amplitude of the fast oscillations is also shown in Fig. 4(c), where the black dashed line denotes the simulation results, its linear fitting is shown by the black solid line with error bar of one standard deviation, and the red line represents the theoretical results. Again, an excellent agreement is obtained. Thus, we provide the physical explanation for the observed HH effects in rapid field variations and describe the temporal development. Some level of space charge, and the existence plasmas and secondary electron emission are identified to be prerequisites for the HH field
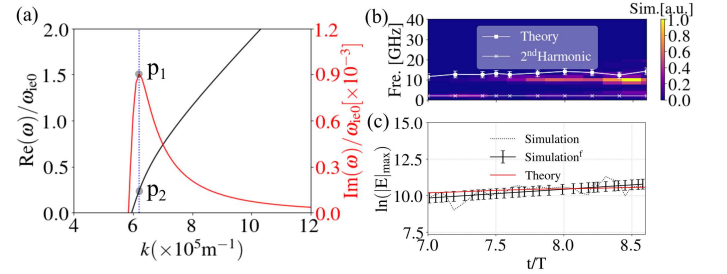

FIG. 4: (a) Theoretical dispersion relationship solution, real and imaginary part of ω, Re(ω) (black line) and Im(ω) (red line), versus k, and the blue dashed line indicates the maximum Im(ω). (b) The time varying frequency spectrum (color bar from simulation) of the normal electric field E_x over time range of 7.0–8.6 rf periods. The color bar gives the relative strength of the magnitude of the Fourier transform of the normal electric field. The time window is 64% of the rf period, with a 78% overlap between successive windows. The white rectangle line shows the theoretical calculation oscillation frequency. (c) The amplitude of the fast oscillation as a function of time in simulation (black dashed line), its linear fitting (black line) and theory (red line).

development. Meanwhile, the observation of HH is connected with electron motion, which is of importance for the fundamental understanding of similar phenomenon in various plasma fields. In addition, the spectrum around 20-25 GHz with much weaker strength, is also observed in the simulation (not shown here), which may be attributed to the second and higher order nonlinearities, and is neglected in the current theory.

In summary, we studied the HH generation of the longitudinal physical quantities normal to the surface, including the normal electric field, electron density etc, in the early stage of multipactor induced plasma breakdown, which are observed for the first time. The theoretical model constructed indicates that stream plasma interaction-induced instability is the mechanism of HH generation in the collisional regime. The excellent agreement between simulation and theory provides a strong basis in understanding the transient physics of breakdown process, which is a crucial step when researchers aim to control it. The regime may be applied to generate a new mode of rf signal, and develop a field frequency spectrum-based new form of diagnostics of the transient plasma behaviors in sub-nanosecond resolution, which is very challenging in the past. This fundamental physics phenomenon can also affect the realistic plasma breakdown process [31, 57, 58]. We emphasize that this phenomenon of HHs is found for Argon, Helium, as well as Xenon, and in a wide range of rf electric field amplitudes and gas pressures, and the present work lays the foundation for future systematic research of the HH oscillations. The HH oscillations are expected to vary for different dielectric materials and SEY coatings, rf frequencies, as well as electronegative gases such as SF_6 used for microwave transmission and space-based satellite communication systems.

The HH generation and its regime revealed in this Letter is not limited to multipactor/plasma discharges, it also shows significance for other systems in the presence of intense secondary electron emission near a surface. The physics reported here may be a good candidate to explain the fast oscillations with short period, whose origin is unknown, in space propulsion systems [59], where the secondary electron emission and the oscillations normal to the surface solely depends on the electron energy tangential to the surface. Additionally, fast oscillations relevant to resonance and instability [60–62], which are part of the fundamental physics of electron heating mechanisms in rf plasma sources, were also reported and partially speculated to be induced by the interaction between sheath-accelerated electron stream and thermal bulk plasma electrons [63, 64]. The theoretical approach constructed here for stream-plasma interaction in the collisional regime may be used to identify the fast-oscillating phenomenon there.

[1] R. A. Kishek and Y. Y. Lau, Phys. Rev. Lett. **80**, 193 (1998).

[2] R. A. Kishek and Y. Y. Lau, Phys. Rev. Lett. **75**, 1218 (1995).

[3] J. G. Power, W. Gai, S. H. Gold, A. K. Kinkead, R. Konecny, C. Jing, W. Liu, and Z. Yusof, Phys. Rev. Lett. **92**, 164801 (2004).

[4] M. A. Lieberman and A. J. Lichtenberg, *Principles of Plasma Discharges and Materials Processing* (John Wiely & Sons, New York, New York, 2005), 2nd ed.

[5] V. A. Lisovskiy and V. D. Yegorenkov, J. Phys. D: Appl. Phys **31**, 3349 (1998).

[6] D. Vender, H. B. Smith, and R. W. Boswell, J. Appl. Phys. **80**, 4292 (1996).

[7] Y. Hidaka, E. M. Choi, I. Mastovsky, M. A. Shapiro, J. R. Sirigiri, and R. J. Temkin, Phys. Rev. Lett. **100**, 035003 (2008).

[8] S. C. Schaub, M. A. Shapiro, and R. J. Temkin, Phys. Rev. Lett. **123**, 175001 (2019).

[9] R. A. Kishek, Phys. Rev. Lett. **108**, 035003 (2012).

[10] R. Udiljak, D. Anderson, M. Lisak, V. E. Semenov, and J. Puech, Phys. Plasmas **11**, 5022 (2004).

[11] R. Udiljak, D. Anderson, M. Lisak, V. E. Semenov, and J. Puech, Phys. Plasmas **10**, 4105 (2003).

[12] R. A. Kishek, Y. Y. Lau, L. K. Ang, A. Valfells, and R. M. Gilgenbach, Phys. Plasmas **5**, 2120 (1998).

[13] A. Valfells, L. K. Ang, Y. Y. Lau, and R. M. Gilgenbach, Phys. Plasmas **7**, 750 (2000).

[14] A. Sazontov, V. Semenov, M. Buyanova, N. Vdovicheva, D. Anderson, M. Lisak, J.Puech, and L. Lapierre, Phys. Plasmas **12** (2005).

[15] C. Chang, M. Zhu, J. Verboncoeur, S. Li, J. Xie, K. Yan, T. Luo, and X. Zhu, Appl. Phys. Lett. **104**, 253504 (2014).

[16] A. Iqbal, J. Verboncoeur, and P. Zhang, Phys. Plasmas **25**, 043501 (2018).

[17] H. Wang, D. Liu, L. Liu, M. Xie, and L. Meng, Plasma Sources Sci. Technol. **27**, 125006 (2018).

[18] H. C. Kim and J. P. Verboncoeur, Phys. Plasmas **12**, 123504 (2005).

[19] A. Iqbal, J. Verboncoeur, and P. Zhang, Phys. Plasmas **26**, 024503 (2019).

[20] D.-Q. Wen, P. Zhang, Y. Fu, J. Krek, and J. P. Verboncoeur, Phys. Plasmas **26**, 123509 (2019).

[21] S. Michizono, Y. Saito, S. Yamaguchi, and S. Anami, IEEE Trans. Electr. Insul. **28**, 692 (1993).

[22] A. Neuber, G. Edmiston, J. Krile, H. Krompholz, J. Dickens, and M. Kristiansen, IEEE Trans. Magn. **43**, 496 (2007).

[23] J. Foster, M. Thomas, and A. Neuber, J. Appl. Phys. **106**, 063310 (2009).

[24] C. Chang, G. Liu, C. Tang, C. Chen, H. Shao, and W. Huang, Appl. Phys. Lett. **96**, 111502 (2010).

[25] D.-Q. Wen, A. Iqbal, P. Zhang, and J. P. Verboncoeur, Phys. Plasmas **26**, 093503 (2019).

[26] P. Zhang, Y. Y. Lau, M. Franzi, and R. M. Gilgenbach, Phys. Plasmas **18**, 053508 (2011).

[27] H. C. Kim and J. P. Verboncoeur, Phys. Plasmas **13**, 123506 (2006).

[28] S. K. Nam and J. P. Verboncoeur, Phys. Rev. Lett. **103**, 055004 (2009).

[29] J.-P. Boeuf, B. Chaudhury, and G. Q. Zhu, Phys. Rev. Lett. **104**, 015002 (2010).

[30] D.-Q. Wen, P. Zhang, J. Krek, Y. Fu, and J. P. Verboncoeur, Appl. Phys. Lett. **119**, 264102 (2021).

[31] Y. Y. Lau, J. P. Verboncoeur, and H. C. Kim, Appl. Phys. Lett. **89**, 261501 (2006).

[32] J. T. Gudmundsson, E. Kawamura, and M. A. Lieberman, Plasma Sources Sci. Technol **22**, 035011 (2013).

[33] D.-Q. Wen, J. Krek, J. T. Gudmundsson, E. Kawamura, M. A. Lieberman, and J. P. Verboncoeur, Plasma Sources Sci. Technol. **30**, 105009 (2021).

[34] A. Iqbal, P. Y. Wong, D.-Q. Wen, J. P. Verboncoeur, and P. Zhang, IEEE Transactions on Plasma Science **49**, 3284 (2021).

[35] V. Vahedi, C. K. Birdsall, M. A. Lieberman, G. DiPeso,

and T. D. Rognlien, Plasma Sources Sci. Technol **2**, 273 (1993).

[36] J. Zhang, W. Luo, M. Jiang, H. Wang, Y. Li, and C. Liu, Plasma Sources Sci. Technol. **29**, 025013 (2020).

[37] V. Vahedi and M. Surendra, Comput. Phys. Comm. **87**, 179 (1995).

[38] J. P. Verboncoeur, Plasma Phys. Control. Fusion **47**, A231 (2005).

[39] J. T. Gudmundsson and M. A. Lieberman, Phys. Rev. Lett. **107**, 045002 (2011).

[40] S. Biagi, www.lxcat.net/Biagi-v7.1. (2004).

[41] M. Hayashi, www.lxcat.net/hayashi. (2019).

[42] E. Eggarter, J. Chem. Phys. **62**, 833 (1975).

[43] D. Vikor, M. Minic, I. Cadez, and M. Kurepa, Fizika **21**, 345 (1989).

[44] A. V. Phelps, J. Appl. Phys. **76**, 747 (1994).

[45] A. V. Phelps and Z. L. Petrovic, Plasma Sources Sci. Technol **8**, R21 (1999).

[46] M. Radmilovi and Z. L. Petrovi, Eur. Phys. J. Appl. Phys. **11**, 3542 (2000).

[47] J. R. M. Vaughan, IEEE Trans. Electron Devices **40**, 830 (1993).

[48] A. Iqbal, P. Y. Wong, J. P. Verboncoeur, and P. Zhang, IEEE Trans. Plasma Sci., **48**, 1950 (2020).

[49] P. Y. Wong, Y. Y. Lau, P. Zhang, N. Jordan, R. M. Gilgenbach, and J. Verboncoeur, Phys. Plasmas **26**, 112114 (2019).

[50] M. Surendra and M. Dalvie, Phys. Rev. E **48**, 3914 (1993).

[51] J. Schulze, Z. Donkó, T. Lafleur, S. Wilczek, and R. P. Brinkmann, Plasma Sources Sci. Technol. **27**, 055010 (2018).

[52] D. Sydorenko, I. D. Kaganovich, P. L. G. Ventzek, and L. Chen, Phys. Plasmas **23**, 122119 (2016).

[53] I. D. Kaganovich and D. Sydorenko, Phys. Plasmas **23**, 112116 (2016).

[54] C. Birdsall and A. Langdon, *Plasma Physics via Computer Simulation* (Institute of Physics, 2004), 2nd ed.

[55] R. Lucken, A. Bourdon, M. A. Lieberman, and P. Chabert, Phys. Plasmas **26**, 070702 (2019).

[56] D. A. Yager-Elorriaga, P. Zhang, A. M. Steiner, N. M. Jordan, P. C. Campbell, Y. Y. Lau, and R. M. Gilgenbach, Phys. Plasmas **23**, 124502 (2016).

[57] M. Puač, D. Marić, M. Radmilović-Radjenović, M. Šuvakov, and Z. L. Petrović, Plasma Sources Sci. Technol. **27**, 075013 (2018).

[58] V. Lisovskiy, J.-P. Booth, K. Landry, D. Douai, V. Cassagne, and V. Yegorenkov, EPL (Europhysics Letters) **82**, 15001 (2008).

[59] M. D. Campanell, A. V. Khrabrov, and I. D. Kaganovich, Phys. Rev. Lett. **108**, 235001 (2012).

[60] S. Wilczek, J. Trieschmann, D. Eremin, R. P. Brinkmann, J. Schulze, E. Schuengel, A. Derzsi, I. Korolov, P. Hartmann, Z. Donk, et al., Physics of Plasmas **23**, 063514 (2016).

[61] E. Schngel, S. Brandt, Z. Donkó, I. Korolov, A. Derzsi, and J. Schulze, Plasma Souce Sci. Technol **24**, 044009 (2015).

[62] S. Sharma, N. Sirse, A. Kuley, and M. M. Turner, Plasma Sources Sci. Technol **29**, 045003 (2020).

[63] J. T. Gudmundsson and D. I. Snorrason, J. Appl. Phys. **122**, 193302 (2017).

[64] A. Meige, D. O'Connell, T. Gans, and R. W. Boswell, IEEE Trans. Plasma Sci. **36**, 1384 (2008).